

## Biological insights of a chiral hybrid-based $\gamma$ -octa-molybdate and proline

Morteza Tahmasebi <sup>a</sup>, Masoud Mirzaei <sup>a,\*</sup>, Maryam M. Matin <sup>b,c,\*</sup>, Sonia Iranpour <sup>b</sup>, Joel T. Mague <sup>d</sup>

<sup>a</sup> Department of Chemistry, Faculty of Science, Ferdowsi University of Mashhad, Mashhad, Iran

<sup>b</sup> Department of Biology, Faculty of Science, Ferdowsi University of Mashhad, Mashhad, Iran

<sup>c</sup> Novel Diagnostics and Therapeutics Research Group, Institute of Biotechnology, Ferdowsi University of Mashhad, Mashhad, Iran

<sup>d</sup> Department of Chemistry, Tulane University, New Orleans, LA 70118, United States

### ARTICLE INFO

#### Article history:

Received 9 August 2021

Received in revised form 26 August 2021

Accepted 29 August 2021

#### Keywords:

Poly-oxometalate

Octamolybdate

Chirality

Coordination polymer

Anti-cancer activity

### ABSTRACT

A new inorganic–organic hybrid based on proline functionalized  $\gamma$ -octamolybdate,  $[\text{Co}_2(\text{H}_2\text{O})_6(\text{Hpro})_2(\text{Mo}_8\text{O}_{26})] \cdot 2\text{H}_2\text{O}$  (1), (pro =  $\text{C}_5\text{H}_9\text{NO}_2$ ) was synthesized under hydrothermal conditions from the reaction of an Evans–Showell-type poly-oxometalate  $(\text{NH}_4)_6[\text{Co}_2\text{Mo}_{10}\text{H}_4\text{O}_{38}]$ , and pro-line. Hybrid 1 was characterized by infrared spectroscopy (IR), elemental analysis, diffuse reflectance spectroscopy (DRS) and single crystal X-ray diffraction methods. As a result, the molecule loses its symmetry and in the molecular state and in the crystalline phase, a chiral structure is obtained. The structure of proline allows the cobalt ion to not only have a covalent interaction with proline via the carboxyl group of proline, but also to act as a linker between two isopoles, leading to a covalent chain. Then, adjacent 1-D chiral chains joined together by another Co–O covalent interaction to yield a 2-D supramolecular chiral layer. The topology of 1, can be rationalized as a two dimensional square lattice (*sql*) coordination network with point symbol  $\{4^2.6^4\}_2\{4^8.6^6.8\}$  in which,  $[\text{Mo}_8\text{O}_{26}(\text{Hpro})_2]^{4-}$  units act as linkers and the Co cations as nodes. Nonetheless, proline ligands have no direct role in expanding the structure as a 2-D covalent polymer. Anti-cancer activity of 1 and two other hybrids were also evaluated to determine the  $\text{IC}_{50}$  values against human-derived colon cancer and normal fibroblast cells. According to the results 1 exhibited significantly higher cytotoxic effects on the cancerous cells in a concentration- and time-dependent manner.

© 2021

### 1. Introduction

Polyoxometalates (POMs) are a class of transition-metal oxide clusters, which possess a large range of structures in terms of size, shape, elemental composition and nuclearities. These enormous structural varieties together with varied redox properties [1–5], make them attractive in various research areas, including biology, magnetism, catalysis and materials science [6–13]. Generally, POMs can be represented by the formula  $(\text{M}_m\text{O}_y)^{x-}$  [isopolyanions (IPA)] and  $(\text{X}_n\text{M}_m\text{O}_y)^{x-}$  [heteropolyanion (HPA)], where  $M = \text{W}, \text{Mo}, \text{V}$  and  $\text{Nb}$  in the highest oxidation state, while  $X$  is a heteroatom. Therefore, IPA contain only transition metals and among them, molybdenum and tungsten are more abundant. Molybdenum in its high oxidation state can form diverse IPA structures such as  $[\text{Mo}_2\text{O}_7]$ ,  $[\text{Mo}_3\text{O}_{10}]$ ,  $[\text{Mo}_4\text{O}_{13}]$ ,  $[\text{Mo}_6\text{O}_{19}]$ ,  $[\text{Mo}_8\text{O}_{26}]$ , etc. [14]. The octamolybdate IPA is a remarkable member of them and has been found in nine isomer forms, namely, the  $\alpha$ ,  $\beta$ ,  $\gamma$ ,  $\delta$ ,  $\epsilon$ ,  $\zeta$ ,  $\xi$ ,  $\eta$  and  $\theta$  isomers [15], with the  $\alpha$ ,  $\beta$  &  $\gamma$  forms more commonly found. Octa-

molybdates can provide plenty of terminal or bridge oxygen atoms. There are four kinds of O atoms in the  $\gamma$ - $[\text{Mo}_8\text{O}_{26}]^{4-}$  anion: terminal O (Ot),  $\mu_2$ —O,  $\mu_3$ —O and  $\mu_4$ —O [16]. Furthermore, both terminal and bridging oxygen atoms can be modified by different species including ionic metal, organic ligand and metal-organic complexes and lead to the generation of multifunctional inorganic-organic hybrid compounds. Interactions between the organic and inorganic parts of the hybrids are divided into two categories. In one category, the interactions, may be weak and include electrostatic interactions, hydrogen bonds or van der Waals interactions. In another category, moieties in hybrids are linked together via strong covalent or ionic-covalent bonds [17]. Moreover, the covalently attached organic ligands offer additional advantages including better POM based stability and desirable ligand orientation, giving novel functions or properties to the POM hybrids. The organic ligands, via O or N donor atoms, can substitute for an oxo group of the POM to be directly linked to a metal center of the POM. Also, metal ions present in the reaction medium, due to the covalent bond, are connected to the electron-rich oxygen atoms. The combination of an octamolybdate cluster and coordination complex fragments with significant structural features might produce some interesting compounds with special physico-chemical properties. Moreover, a hybrid containing in-

\* Corresponding authors.

E-mail addresses: [mirzaesh@um.ac.ir](mailto:mirzaesh@um.ac.ir) (M. Mirzaei), [matin@um.ac.ir](mailto:matin@um.ac.ir) (M.M. Matin).

organic and organic parts, with repeating coordination entities extending in 1, 2, or 3 dimensions, can create a coordination polymer. One of the most significant potential modifications of POMs is the reduction of the initial high symmetry to generate low-symmetry hybrids based on POMs. In the absence of a symmetry plane, chiral structures may result which have properties quite different from achiral structures. It is well known that most POM clusters possess high symmetry and there are very few chiral compounds in which the chirality is due to their inherent structure. Thus, the symmetry in these compounds must be broken by creating a vacant compound by the removal of one or several metal atoms or by substitution with different metal or other atoms. Examples of the latter are chiral POM anions, such as  $[P_2W_{17}O_{61}]^{10-}$  [18] and  $[SiW_{11}O_{39}]^{8-}$  [19]. In others, the chirality is obtained from alternating bond lengths, as in  $[MnMo_9O_{32}]^{6-}$  [20] and  $[P_2Mo_{18}O_{62}]^{6-}$  [21]. Finally, one can add organic ligands to remove the inversion or mirror symmetry in POMs. Generally, chiral POM-based compounds can be obtained by two routes. The first method is based on the use of chiral species, including chiral organic molecules, chiral metal-organic units or chiral POMs as structure-directing agents. Here, the chirality of substances can be transferred to the whole structure by using dissymmetric species, by the bonding of the metal centers to the POM cluster or by hydrogen-bond interactions [22–24]. This method has been a considerable development [25–27]. An example of this method is a chiral hybrid that is constructed from  $[CoMo_6O_{24}]^{6-}$  clusters and histidine in which the chirality of the amino acid is transferred to the whole framework through the bonding of chiral histidine to the POM cluster [28].

In another example, the use of an Evans–Showell POM cluster as a chiral polyoxoanion transfers its chirality to the whole framework [29]. In most cases, the use of chiral ligands to synthesize a chiral hybrid is more common because of their diversity and abundance. The second method for creating chiral compounds is the use of achiral starting materials, which undergo spontaneous resolution without any chiral auxiliary [30]. Spontaneous resolution is one of the oldest and most fascinating but challenging methods to prepare chiral POMs. On the basis of results to date, it is found that destroying the symmetry of achiral starting species during the assembly process should be a key factor. However, to increase the predictability of preparing chiral conglomerates by this method the starting species should have chiral building units. Most reports focused on amino acid ligands coordinating to POMs directly via covalent interaction. However, very rare hybrids constructed from POMs and amino acid-metal (metal-organic) fragments have been reported [31,32]. In this work, an inorganic-organic hybrid based on  $\gamma$ -octamolybdate (Fig. 1) has been synthesized under hydrothermal con-

dition using  $[Co_2Mo_{10}H_4O_{38}]^{6-}$  and L-proline. The building blocks are linked via strong covalent bonds so that proline acts as a bridge between two metallic centers (Mo and Co). Finally, the resulting hybrid is expanded in two dimensions by covalent bonds, resulting in a coordination polymer. In recent years there has been a growing interest in the biological activity of POMs. Studies on POMs have indicated their tumor growth inhibition properties [33–37]. For example, anti-tumor activities for  $[NH_3Pr^I]_6[Mo_7O_{24}] \cdot 3H_2O$  [38],  $[NH_4]_{17}Na[NaSb_9W_{21}O_{86}] \cdot 14H_2O$  [39], and  $Na[IMo_6O_{24}]$  [40] were reported against various cancer cells. Furthermore, it is noteworthy that, the presence of cobalt and molybdenum in the hybrid is more important [41,42]. The only mechanism for the anti-tumoral activity of POMs that was proposed by Yamase revolves around a single electron reduction/oxidation cycle in isopolymolybdates [43]. In this study, the anti-cancer activities of 1 along with two other hybrids,  $[Co_2(C_4H_6NO_4)_2(\gamma-Mo_8O_{26})(H_2O)_{10}] \cdot 4H_2O$  (2) [16] and  $NH_4[Mo_2(C_6H_{11}O_6)_5]H_2O$  (3) [44] were evaluated to determine the  $IC_{50}$  values against two human-derived cell lines, LoVo colon cancer cells as well as normal fibroblasts.

## 2. Experimental

### 2.1. Materials and methods

$(NH_4)_6[Co_2Mo_{10}H_4O_{38}] \cdot 7H_2O$  was synthesized according to the literature [45] and was characterized by IR spectroscopy. All other reagents and solvents were purchased from commercial sources and used without further purification. IR spectra were recorded as KBr pellets on a Buck 500 IR spectrometer in the range 4000–400  $cm^{-1}$ . UV–vis diffuse reflective spectroscopy was conducted in the wavelength range 200–800 nm using a Scinco S400 spectrophotometer. The C, H and N elemental analyses were performed on a Thermo Finnigan Flash model 1112EA micro analyzer. Powder X-ray diffraction (PXRD) data were collected on ASENWARE/AW-XDM300 X-ray powder diffractometer using  $Cu K\alpha$  ( $\lambda = 1.54184 \text{ \AA}$ ) radiation at room temperature with the scan range  $2\theta = 5$  to  $50^\circ$  and step size of  $0.05^\circ$  and step time of 1 s. X'Pert HighScore Plus was used to compare the experimental PXRD pattern with the simulated lines from the crystal structure.

### 2.2. Synthesis of 1

Enantiopure L-proline (0.047 g, 0.4 mmol) was dissolved in water (7 mL) and ethanol (3 mL) was added, resulting in a pH of the solution above 4. An aqueous solution (8 mL) of  $(NH_4)_6[Co_2Mo_{10}H_4O_{38}] \cdot 7H_2O$  (0.2 g, 0.1 mmol) was added drop wise to the first solution leading to a solution pH of 4.5. The resulting solution was stirred for 2 h in 70 °C and then transferred to a Teflon-lined autoclave (30 mL) and kept at 110 °C for 72 h. After the mixture had been cooled slowly to room temperature, the solution was filtered and, after a few days, pale-orange crystals were obtained in 54% yield (based on Mo). Elemental Anal. Found (Calcd%): C, 7.15 (7.17); H, 2.11 (2.05); N, 1.63 (1.67). IR (KBr pellet,  $cm^{-1}$ ): 3541(s), 3407(w), 2850(w), 1622(s), 1561(m), 1427(m), 1167(w), 936(s), 898(m), 838(w) and 700(s).

### 2.3. X-ray crystallography

A pale-orange single crystal of 1 was used for the X-ray crystallographic analysis. The X-ray intensity data were collected on a Bruker Smart APEX CCD system equipped with a graphite mono chromator. Crystallographic data were collected at temperature of 150(2) K to a maximum  $2\theta$  value of  $64.146^\circ$  and integrated using the Bruker SAINT Software package using a narrow-frame algorithm. Data were corrected for absorption effects using the multi-scan method (SADABS). The structure was solved by direct methods (SHELXT) and refined F2 by fullmatrix least-squares method using the SHELXL-2014/7 program

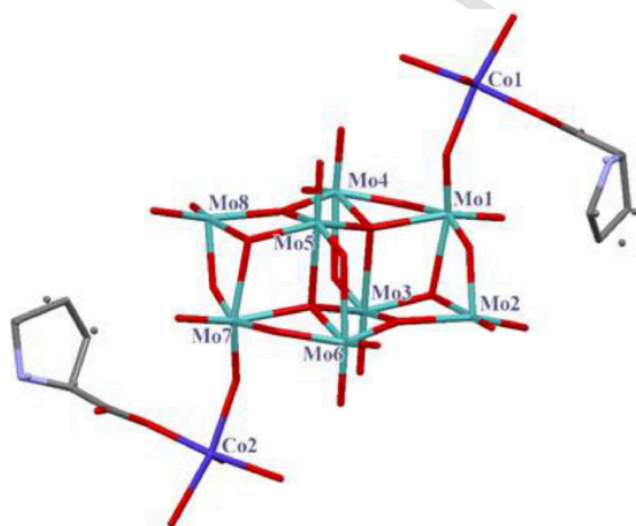


Fig 1. A view of the asymmetric unit of 1. All H atoms and uncoordinated water molecules have been omitted for clarity.

package [46–49]. A summary of refinement parameters can be seen in Table 1.

## 2.4. Anti-cancer activity study

### 2.4.1. Solution preparation

Two mg of hybrids 1, 2 and 3 were dissolved in 100  $\mu$ l of hydrochloric acid (HCl 0.3 N) to make a primary stock solution. Different concentrations (3.125–100  $\mu$ g/ml) were then prepared by serial dilution with culture medium. The formula and molecular weights of each hybrid was as follows: hybrid 1  $[\text{Co}_2(\text{H}_2\text{O})_6(\text{Hpro})_2(\text{Mo}_8\text{O}_{26})] \cdot 2\text{H}_2\text{O}$ , MW = 1674 g/mol; hybrid 2  $[\text{Co}_2(\text{C}_4\text{H}_6\text{NO}_4)_2(\gamma\text{-Mo}_8\text{O}_{26})(\text{H}_2\text{O})_{10}] \cdot 4\text{H}_2\text{O}$ , MW = 1818 g/mol, and hybrid 3  $\text{NH}_4[\text{Mo}_2(\text{C}_6\text{H}_{11}\text{O}_6)\text{O}_5] \cdot \text{H}_2\text{O}$ , MW = 488 g/mol.

### 2.4.2. Cell culture

Human colon cancer cells (LoVo) and human dermal fibroblast cells (HDF) were selected in order to determine the toxicity and safety of the mentioned compounds. In this context, LoVo cells were cultured in Roswell Park Memorial Institute medium (RPMI 1640; Gibco, Scotland), supplemented with 10% fetal bovine serum (FBS; Gibco, Brazil). HDF cells were kindly provided by Academic Center for Education, Culture and Research (ACECR, Mashhad, Iran) and cultured in Dulbecco's modified Eagle's medium (DMEM; Gibco, Scotland) containing 10% FBS and antibiotics (100  $\mu$ g/ml streptomycin and 100 U/ml penicillin; Gibco, UK). Both cell lines were maintained in a humidified atmosphere of 5%  $\text{CO}_2$  at 37  $^\circ\text{C}$  and passaged as required.

### 2.4.3. MTT assay

Cytotoxic effects of tested hybrids were determined by MTT (3-(4,5-dimethylthiazol-2-yl)-2,5-diphenyltetrazolium bromide) assay (Tinab Shimi, Iran) according to the original protocol described for the first time by Mosmann [50], which was optimized for our cell lines. To do so, LoVo and HDF cells were seeded in 96-well plates (SPL Life Sciences, Korea), at densities of 6000 and 8000 cells/well, respectively. After 24 h, the media were replaced with fresh media containing different concentrations (3.125–100  $\mu$ g/ml) of desired compounds and incubated for 24, 48, and 72 h at 37  $^\circ\text{C}$  and 5%  $\text{CO}_2$ . 20  $\mu$ l MTT solution was then added to the wells and incubated for 3–4 h at 37  $^\circ\text{C}$  in dark condi-

tions. The media were then replaced with 160  $\mu$ l dimethyl sulfoxide (DMSO) and absorbance of each well was measured at 545 nm using an enzyme-linked immunosorbent assay (ELISA) reader (Awareness Technology, USA). Experiments were performed in triplicate for all treatments. Finally, statistical analyses were carried out using GraphPad Prism software 6.0 (San Diego, USA). The differences between groups were assessed with Student's *t*-test (group pairs) followed by Tukey multiple comparison tests.

## 3. Results and discussion

### 3.1. Synthesis

The Evans–Showell type POM, after reaction at high temperatures can often turn into the Anderson form [26], or  $\gamma$ -octamolybdate IPA and  $\text{Mo}_2\text{O}_5$  fragment anions [44]. In the present instance, the heteropolyanion is converted to octamolybdate under hydrothermal conditions, and its Co atoms, coordinated by proline and three water molecules coordinated by two adjacent octamolybdate anions.

### 3.2. Crystal structure of 1

The asymmetric unit consists of a  $\gamma$ -octamolybdate anion ( $[\text{Mo}_8\text{O}_{26}]^{4-}$ ) two crystallographically independent Co(II) ions two crystallographically unique proline ligands, six coordinated and two uncoordinated water molecules. The five-membered rings of both proline molecules are disordered over two sites involving different ring conformations (0.51(1):0.49(1) for that on Co1 and 0.70(1):0.30(1) for that on Co2) but the chirality of the ligands is unaffected. The  $\gamma$ -octamolybdate anion, is connected to the two bondunique cobalt ions via coordination of the terminal Mo = O units Mo1 = O1 (to Co1) and Mo7 = O22 (to Co2) (Fig. 1). The  $\gamma$ - $[\text{Mo}_8\text{O}_{26}]^{4-}$  anion is built up of six distorted edge-shared  $\{\text{MoO}_6\}$  octahedra and two distorted square-pyramidal  $\{\text{MoO}_5\}$  subunits (Fig. 2a,b). The two five-coordinated Mo atoms (Mo2 and Mo8), placed at opposite ends of the  $\gamma$ -octamolybdate IPA, are further coordinated by an O atom from proline ligand, (O31<sup>i</sup>–Mo2, O36<sup>ii</sup>–Mo8 with symmetry codes: (i)  $-x + 1, y - 1/2, -z + 1$ ;

**Table 1**  
X-ray diffraction crystallographic data and structure refinements for 1.

Chemical formula	$\text{C}_{10}\text{H}_{30}\text{Co}_2\text{Mo}_8\text{N}_2\text{O}_{36} \cdot 2(\text{H}_2\text{O})$
$M_r$ ( $\text{g mol}^{-1}$ )	1675.77
Crystal system, space group	Monoclinic, $P2_1$
Temperature (K)	150
$a, b, c$ ( $\text{\AA}$ )	11.7603 (9), 13.3102 (11), 12.703 (1)
$\beta$ ( $^\circ$ )	103.981 (2)
$V$ ( $\text{\AA}^3$ )	1929.5 (3)
$Z$	2
Radiation type	Mo $K\alpha$
$\mu$ ( $\text{mm}^{-1}$ )	3.47
Crystal size (mm)	$0.12 \times 0.12 \times 0.10$
$T_{\text{min}}, T_{\text{max}}$	0.65, 0.72
$R_{\text{int}}$	0.027
$(\sin \theta/\lambda)_{\text{max}}$ ( $\text{\AA}^{-1}$ )	0.747
$R[F^2 > 2\sigma(F^2)], wR(F^2), S$	0.021, 0.043, 1.08
No. of reflections	13,447
CCDC number	2,091,124
No. of parameters	580
No. of restraints	87
$\Delta\rho_{\text{max}}, \Delta\rho_{\text{min}}$ ( $\text{e \AA}^{-3}$ )	0.63, $-0.91$
Absolute structure	Refined as an inversion twin.
Absolute structure parameter	0.037 (18)

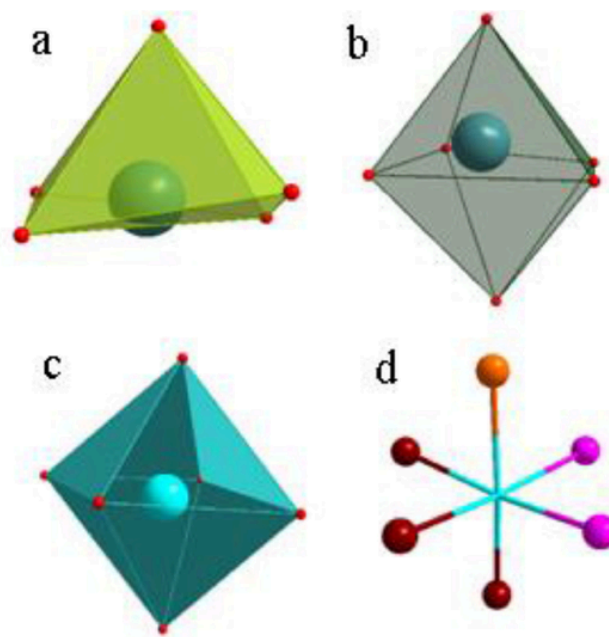


**Fig 2.** a) A polyhedra view of the octahedral coordination of  $\text{Co}^{\text{II}}$ . b) Coordination geometry around the  $\text{Co}^{\text{II}}$  center. Color code: O atom from carboxylic acid group = orange, O atoms from IPA = pink; O atoms from water ligands = dark red.

(ii)  $-x + 2, y + \frac{1}{2}, -z$ ), thereby satisfying the octahedral coordination of all the Mo atoms (Fig. S1a,b). There are four kinds of O atoms in the  $\gamma$ -[Mo<sub>8</sub>O<sub>26</sub>]<sup>4-</sup> anion: terminal O (Ot),  $\mu_2$ -O,  $\mu_3$ -O and  $\mu_4$ -O. In each anion, there are 14 terminal Ot, six  $\mu_2$ -O, four  $\mu_3$ -O and two  $\mu_4$ -O atoms. While Fig. 1 suggests a centrosymmetric structure for 1, as is the case for the  $\gamma$ -[Mo<sub>8</sub>O<sub>26</sub>]<sup>4-</sup> anion itself, trial refinements in both the centric and non-centric space groups resulted in considerably better results in the latter in terms of a lower value for R1, the ability to locate many hydrogen atoms in a difference map and, particularly, lower residual peaks in the final difference map and well-behaved displacement ellipsoids except for the disordered atoms. On these bases, we conclude that 1, is not centro symmetric and this is reflected in statistically different values for pairs of bond lengths which would be identical under the higher symmetry. For example, the Mo2–O4 (2.307(3) Å) and Mo8–O16 (2.267(3) Å) differ by 13 $\sigma$  while the Mo3–O4 and Mo5–O16 distances (1.899(3) and 1.925(3) Å, respectively) differ by 9 $\sigma$ . Similarly, the non-bonded distances Mo1...Mo4 (3.2567(6) Å) and Mo6...Mo7 (3.2358(6) Å) differ by 35 $\sigma$  while the Mo1...Mo3 (3.4549(6) Å) and Mo5...Mo7 (3.4661(6) Å) distances differ by 19 $\sigma$  while the Co1–O1 (2.058(4) Å) and Co2–O22 (2.114(4) Å) bond lengths differ by 14 $\sigma$  and the Mo1–O1 (1.732(4) Å) and Mo7–O22 (1.719(4) Å) bond lengths by just over 3 $\sigma$ . Both Co ions are six-coordinated with distorted octahedral geometry being surrounded by three O atoms from water ligands, an O atom from each of two different octamolybdate anions and one O atom from the carboxylic acid group of the proline ligand (Fig. 2d). Each proline ligand is coordinated to one Mo atom of the  $\gamma$ -[Mo<sub>8</sub>O<sub>26</sub>]<sup>4-</sup> anion and one Co<sup>II</sup> cation through its carboxyl oxygen atoms. To maintain charge balance, two protons were added to the formula. Because of the disorder, it is not clear from difference maps if the proline nitrogens are protonated, but these are the likely sites as the difference map remained basically flat after adding the extra protons to nitrogen but adding them to other sites on the anion generated definite areas of negative density where the hydrogens were placed. The {Co(H<sub>2</sub>O)<sub>3</sub>(Hpro)} units thus serve to expand the structure into a 2-D layer coordination polymer. Examples of high-dimensional hybrids based on  $\gamma$ -[Mo<sub>8</sub>O<sub>26</sub>]<sup>4-</sup>, especially with amino acid ligands, have rarely been reported, and it appears that, the type of metal atom and organic

ligand plays a decisive role in determining the resulting hybrid dimension. For example, a report by the An Group [51] shows that reacting the POM and lysine with copper ions leads to a two-dimensional product. However, when cobalt was used in place of copper, 0-D structures were obtained owing to the different coordination modes of the Cu<sup>II</sup> and Co<sup>II</sup> cations. As an example of the influence of the ligand, in our previous work, in the presence of the same POM and metal ions as in the present work, but with aspartic acid as a ligand, an iso-structural 0-D structure was obtained.

An alternate description of the structure of the solid has the chiral subunits [Mo<sub>8</sub>O<sub>26</sub>(Hpro)<sub>2</sub>]<sup>4-</sup> linked by Co–O covalent interactions to form 1-D supra-molecular chiral chains (Fig. S2). These 1-D chiral chains are joined via other Co cations to form a 2-D layer (Fig. S3). Adjacent 2-D planes are linked together by strong hydrogen-bonding interactions (O21...O28, O32...O5, O25...O5, O32...O28, O25...O28, N1...O25, C7...O19) to generate an interesting 3-D supra-molecular network (Figs. 3b and S4). To gain better insight into the 2-D framework structure, a topological analysis was carried out. The topology of 1, can be rationalized as a two-dimensional sql coordination network with point symbol {4<sup>2</sup>.6<sup>4</sup>}<sub>2</sub>{4<sup>8</sup>.6<sup>6</sup>.8}. The 2-D framework is a common 4-connected 4<sup>4</sup> net with [Mo<sub>8</sub>O<sub>26</sub>(Hpro)<sub>2</sub>]<sup>4-</sup> units as linkers and the Co cations as nodes. However, the proline ligands have no direct role in expanding the structure as a 2-D covalent polymer (Fig. 3c). Besides these covalent interactions, strong hydrogen-bonding interactions stabilize the layered structural arrangement.

### 3.3. PXRD analysis

The purity of crystals of the hybrid was verified by powder X-ray diffraction. Therefore, as a result, the relative intensities of all peaks are those expected based on the simulated diffraction pattern of the bulk powder, as shown in Fig. S5.

### 3.4. IR spectroscopy

The IR spectrum of 1 (Fig. S6) has the characteristic asymmetric stretching vibration bonds at 936, 898, 838 and 700 cm<sup>-1</sup> confirming

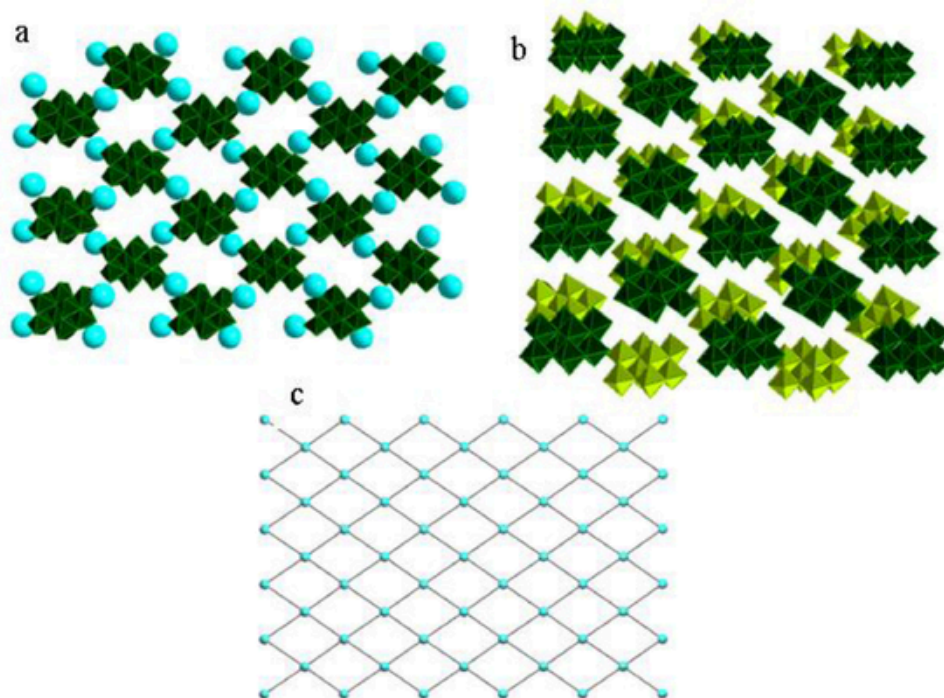


**Fig 3.** a) A polyhedral view of the 2-D CP in 1. B) Polyhedral view of the 3-D supra-molecular framework of 1 c) Simplified representation of the 3-D network of 1. View along the crystallographic c axis.

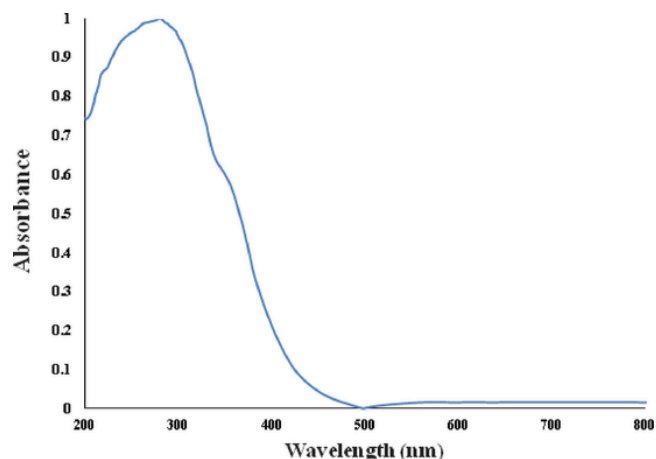


Fig 4. UV–vis diffuse reflectance spectrum of 1.

the presence of Mo—Ot and Mo—Ob (b is bridging) groups. These characteristic bands are nearly identical to those of reported octamolybdate hybrids [52]. The wagging vibration of the  $\omega\text{CH}_2$ , and the scissoring vibrations of the  $\delta\text{CH}_2$  groups appear in the region 1380 and 1560  $\text{cm}^{-1}$  respectively. The band at 1167 is assigned to the CN stretch in proline. The band at 1561  $\text{cm}^{-1}$  is assigned to CH bending in proline. The symmetrical and asymmetrical  $\text{COO}^-$  stretching vibrations are centered at 1427 and 1622  $\text{cm}^{-1}$ , respectively [53]. The absence of CO bands around 1720  $\text{cm}^{-1}$  indicates that all the carboxylic acid groups are deprotonated in 1. The bands located at 2850, 3407 and 3541  $\text{cm}^{-1}$  are assigned to the CH stretching, OH vibration of the uncoordinated and coordinated water molecules, and NH stretching respectively.

### 3.5. UV–vis diffuse reflective spectroscopy

The UV–vis diffuse reflective spectrum for the solid sample in the 200–800 nm region is shown in Fig. 4. The plot displays two absorption bands for O  $\rightarrow$  Mo charge transfer, which is characteristic of POMs. The strong band at 284 nm is attributed to Ot  $\rightarrow$  Mo charge transfer and the weak bands at 353 nm is assigned to the Ob,c  $\rightarrow$  Mo charge transfer and the absorption edge located at 450 nm [54].

### 3.6. Cytotoxicity assay

In present study, anti-cancer properties of desired hybrids were investigated on LoVo and HDF cells by MTT assay. Both cancerous and normal cells were treated with various concentrations (3.125–100  $\mu\text{g}/\text{ml}$ ) of hybrids 1, 2 and 3. After 24, 48, and 72 h, the percentage of cell survival was measured and the  $\text{IC}_{50}$  values for different time points were determined as presented in Table 2. As shown in Fig. 5, treatment with 1 induced a more pronounced time- and dose-dependent decrease in viability of LoVo cells. Our results indicated that LoVo colon cancer cells displayed various sensitivities to hybrids and 1 exhibited the highest toxicity as compared with 2 and 3. Interestingly, significant differences were observed between the cytotoxic effects of tested compounds on cancerous and normal cells as illustrated in Fig. 6. Our results are consistent with other studies showing functionalization of POMs with amino acid is an effective strategy to improve anti-cancer properties of parent molecule. For instance, Chen et al. demonstrated higher anti-cancer activity of Cu- and Zn-directed amino acid functionalized POMs against MCF-7 and HepG2 in comparison with the parent molecule [51]. Moreover, Li et al. reported significant ( $p < 0.05$ ) anti-proliferative effects of two POMs functionalized by glycine on A549 cells as compared with 5-fluorouracil [55].

Table 2

Comparing the  $\text{IC}_{50}$  values of tested hybrids on LoVo and HDF cells during 24, 48, and 72 h of treatments. Data are expressed as mean  $\pm$  SD,  $n = 3$ .

Entry	$\text{IC}_{50}$ ( $\mu\text{M}$ ) $\pm$ SD (LoVo)			$\text{IC}_{50}$ ( $\mu\text{M}$ ) $\pm$ SD (HDF)		
	24 h	48 h	72 h	24 h	48 h	72 h
Hybrid 1	52.09 $\pm$ 1.96	35.19 $\pm$ 1.90	22.02 $\pm$ 1.93	249.4 $\pm$ 2.31	210.2 $\pm$ 2.45	136.37 $\pm$ 2.04
Hybrid 2	149.39 $\pm$ 1.99	134.98 $\pm$ 1.94	115.29 $\pm$ 2.04	1171.61 $\pm$ 3.23	966.99 $\pm$ 3.26	664.4 $\pm$ 3.33
Hybrid 3	447.95 $\pm$ 1.82	329.30 $\pm$ 1.90	245.28 $\pm$ 1.95	872.13 $\pm$ 1.99	734.63 $\pm$ 2.1	616.18 $\pm$ 2.1

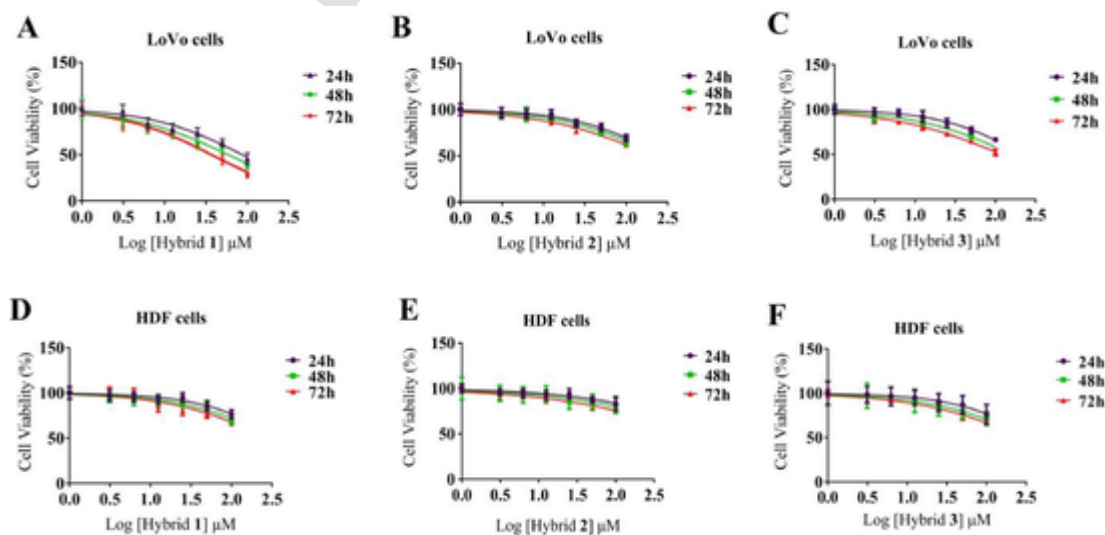


Fig. 5. Dose-response curves indicating the effects of different concentrations of hybrids 1, 2 and 3 on viability of LoVo and HDF cells during 24, 48, and 72 h time intervals. Data are expressed as mean  $\pm$  SD,  $n = 3$ .

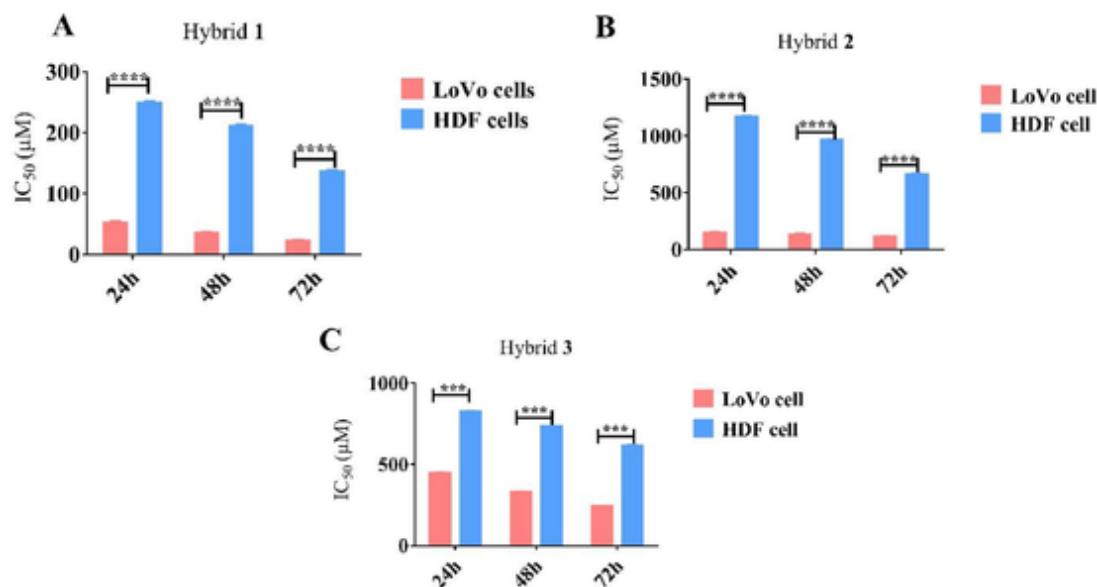


Fig. 6. Comparing the cytotoxic effects of (A) 1, (B) 2, and (C) 3 on LoVo and HDF cells at different time points. Data are expressed as mean  $\pm$  SD,  $n = 3$ , \*\*\*  $p < 0.001$  and \*\*\*\*  $p < 0.0001$ .

#### 4. Conclusions

In conclusion, we report a new 2-D coordination polymer, based on proline functionalized  $\gamma$ -octamolybdate. Expansion of the chiral subunit  $[\text{Mo}_8\text{O}_{26}(\text{Hpro})_2]^{4-}$ , via covalent bonds between the cobalt cation as nodes and an IPA oxygen yielded a two-dimensional covalent polymer. The topology of 1, can be rationalized as a two dimensional sql coordination network with point symbol  $\{4^2.6^4\}_2\{4^8.6^6.8\}$  in which,  $[\text{Mo}_8\text{O}_{26}(\text{Hpro})_2]^{4-}$  units act as linkers and the  $\text{Co}^{\text{II}}$  cations as nodes. 2-D planes are linked together by strong hydrogen-bonding interactions to generate an interesting 3-D supra-molecular network. Furthermore, in this study, the anti-cancer activity of 1 was evaluated to determine the  $\text{IC}_{50}$  values against two human-derived colon cancer and normal fibroblast cells. Hybrid 1 exhibited both concentration- and time-dependent cytotoxic effects on the cancerous cells during 24, 48, and 72 h of administration. Interestingly, it had a significantly less cytotoxicity on HDF normal cells at all-time points ( $p < 0.0001$ ). Since hybrid 1 displayed selective cytotoxic effects on cancer cells, this work might be an initiation point for introducing new therapeutic agents for management of colon cancer. However, further *in vitro* and *in vivo* investigations are needed to verify the stability and also confirm the efficacy of this synthetic hybrid as a valid anti-cancer agent.

#### Authors' contributions

Morteza Tahmasebi: Formal analysis, Data curation, Experimental work performance, Writing-original draft. Masoud Mirzaei: Funding acquisition, Supervision, Main idea, writing-review & editing. Joel T Mague: Crystallographer. Maryam M Matin: Experimental work performance and formal analyses, funding and editing the manuscript. Sonia Iranpour: Experimental work performance and formal analyses.

#### Declaration of Competing Interest

There are no conflicts to declare.

#### Acknowledgements

M.M. gratefully acknowledges financial support from Ferdowsi University of Mashhad (Grant No. 3/44165), the Iran Science Elites Federation (ISEF), Zeolite and Porous Materials Committee of Iranian Chemi-

cal Society and Iran National Science Foundation (INSF). This work is supported by Iran Science Elites Federation Grant No. M/98208, M/99397, and M/400230. M.M. also acknowledge the Cambridge Crystallographic Data center (CCDC) for access to the Cambridge Structural Database. J.T.M. thanks Tulane University for support of the Tulane Crystallography Laboratory. A.F. thanks the MICIU/AEI of Spain (project CTQ2017- 85821-R FEDER funds) for financial support.

#### Supplementary materials

Supplementary material associated with this article can be found, in the online version, at [doi:10.1016/j.molstruc.2021.131401](https://doi.org/10.1016/j.molstruc.2021.131401).

#### References

- [1] M. Hutin, C. Yvon, J. Yan, A. Macdonell, D.-. L. Long, L. Cronin, *Cryst. Eng. Comm.* 15 (2013) 4422–4430.
- [2] Y.-. F. Song, R. Tsunashima, *Chem. Soc. Rev.* 41 (2012) 7384–7402.
- [3] S. Taleghani, M. Mirzaei, H. Eshtiagh-Hosseini, A. Frontera, *Coord. Chem. Rev.* 309 (2016) 84–106.
- [4] M. Tahmasebi, M. Mirzaei, A. Frontera, *Inorg. Chim. Acta* (2021) 120410.
- [5] M. Mirzaei, H. Eshtiagh-Hosseini, M. Alipour, A. Frontera, *Coord. Chem. Rev.* 275 (2014) 1–18.
- [6] A. Müller, F. Peters, M.T. Pope, D. Gatteschi, *Chem. Rev.* 98 (1998).
- [7] N. Mizuno, M. Misono, *Chem. Rev.* 98 (1998) 199–218.
- [8] M. Samaniyan, M. Mirzaei, R. Khajavian, H. Eshtiagh-Hosseini, C. Streb, *ACS Catal* 9 (2019) 10174–10191.
- [9] M.A. Fashapoyeh, M. Mirzaei, H. Eshtiagh-Hosseini, A. Rajagopal, M. Lechner, R. Liu, C. Streb, *Chem. Commun.* 54 (2018) 10427–10430.
- [10] M. Bazargan, F. Ghaemi, A. Amiri, M. Mirzaei, *Coord. Chem. Rev.* 445 (2021) 214107.
- [11] Z. Khoshkhan, M. Mirzaei, H. Eshtiagh-Hosseini, M. Izadyar, J.T. Mague, M. Korabik, *Polyhedron* 194 (2021) 114903.
- [12] X. Wang, Z. Feng, B. Xiao, J. Zhao, H. Ma, Y. Tian, H. Pang, L.J.G.C. Tan, *Green. Chem.* 22 (18) (2020) 6157–6169.
- [13] R. Liu, K. Cao, A.H. Clark, P. Lu, M. Anjass, J. Biskupek, U. Kaiser, G. Zhang, *C.J.C.s. Streb, Chem. Sci.*, 11 (4) (2020) 1043–1051.
- [14] C.-. Z. Lu, C.-. D. Wu, H.-. H. Zhuang, J.-. S. Huang, *Chem. Mater.* 14 (2002) 2649–2655.
- [15] H. Guo, C. Gong, X. Zeng, H. Xu, Q. Zeng, J. Zhang, Z. Zhong, J. Xie, *Dalton Trans* 48 (2019) 5541–5550.
- [16] M. Tahmasebi, M. Mirzaei, H. Eshtiagh-Hosseini, J.T. Mague, A. Bauzá, A. Frontera, *Acta Cryst. C* 75 (2019) 469–477.
- [17] M. Mirzaei, H. Eshtiagh-Hosseini, N. Lotfian, A. Salimi, A. Bauzá, R. Van Deun, R. Decadt, M. Barceló-Oliver, A. Frontera, *Dalton Trans.*, 43 (2014) 1906–1916.
- [18] M. Sadakane, M.H. Dickman, M.T. Pope, *Inorg. Chem.* 40 (2001) 2715–2719.
- [19] U. Kortz, S. Matta, *Inorg. Chem.* 40 (2001) 815–817.
- [20] T. Weakley, *J. Less-Common Met.* 54 (1977) 289–296.
- [21] J.F. Garvey, M.T. Pope, *Inorg. Chem.* 17 (1978) 1115–1118.

- [22] D.-. Y. Du, L.-. K. Yan, Z.-. M. Su, S.-. L. Li, Y.-. Q. Lan, E.-. B. Wang, *Coord. Chem. Rev.* 257 (2013) 702–717.
- [23] Y.-l. Teng, B.-x. Dong, J. Peng, S.-y. Zhang, L. Chen, L. Song, J. Ge, *CrystEngComm* 15 (2013) 2783–2785.
- [24] Y.-. Q. Lan, S.-. L. Li, Z.-. M. Su, K.-. Z. Shao, J.-. F. Ma, X.-. L. Wang, E.-. B. Wang, *Chem. Commun.* (2008) 58–60.
- [25] F. Xin, M.T. Pope, *J. Am. Chem. Soc.* 118 (1996) 7731–7736.
- [26] X. Fang, T.M. Anderson, C.L. Hill, *Angew. Chem. Int. Ed.* 117 (2005) 3606–3610.
- [27] U. Kortz, M.G. Savelieff, F.Y.A. Ghali, L.M. Khalil, S.A. Maalouf, D.I. Sinno, *Angew. Chem. Int. Ed.* 41 (2002) 4070–4073.
- [28] M. Arefian, M. Mirzaei, H. Eshtiagh-Hosseini, *J. Mol. Struct.* 1156 (2018) 550–558.
- [29] H. An, L. Wang, Y. Hu, T. Xu, Y. Hou, *Inorg. Chem.* 55 (2016) 144–153.
- [30] Z.-. M. Zhang, X. Duan, S. Yao, Z. Wang, Z. Lin, Y.-. G. Li, L.-. S. Long, E.-. B. Wang, W. Lin, *Chem. Sci.* 7 (2016) 4220–4229.
- [31] H. Eshtiagh-Hosseini, M. Mirzaei, *J. Clust. Sci.* 23 (2012) 345–355.
- [32] M. Arefian, M. Mirzaei, H. Eshtiagh-Hosseini, A. Frontera, *Dalton Trans* 46 (2017) 6812–6829.
- [33] A. Bijelic, M. Aureliano, A. Rompel, *Angew. Chem. Int. Ed.* 58 (2019) 2980–2999.
- [34] E. Cartuyvels, K. Van Hecke, L. Van Meervelt, C. Görller-Walrand, T.N. Parac-Vogt, *J. Inorg. Biochem.* 102 (2008) 1589–1598.
- [35] L. Wang, B.-. B. Zhou, K. Yu, Z.-. H. Su, S. Gao, L.-. L. Chu, J.-. R. Liu, G.-. Y. Yang, *Inorg. Chem.* 52 (2013) 5119–5127.
- [36] M.S. Hosseini, S.H. Javanmard, N. Dana, L. Rafiee, M. Rostami, *J. Inorg. Organomet. Polym. Mater.* (2021) 1–13.
- [37] J.T. Rhule, C.L. Hill, D.A. Judd, R.F.J.C.R. Schinazi, *Chem. Rev.* 98 (1) (1998) 327–358.
- [38] T. Yamase, H. Fujita, K. Fukushima, *Inorg. Chim. Acta* 151 (1988) 15–18.
- [39] C. Jasmin, N. Raybaud, J. Chermann, D. Haapala, F. Sinoussi, C.B. Loustau, C. Bonissol, P. Kona, M. Raynaud, *Biomedicine (Taipei)* 18 (1973) 319C.
- [40] H. Fujita, T. Fujita, T. Sakurai, T. Yamase, Y. Seto, *Tohoku J. Exp. Med.* 168 (1992) 421–426.
- [41] E. Rauwel, S. Al-Arag, H. Salehi, C.O. Amorim, F. Cuisinier, M. Guha, M.S. Rosario, P. Rauwel, *Int. J. Nanomed* 15 (2020) 7051.
- [42] A.T. Odularu, P.A. Ajibade, J.Z. Mbese, *Bioinorg. Chem. Appl.* 2019 (2019) 1–9.
- [43] T. Yamase, *Mol. Eng.* 3 (1993) 241–262.
- [44] M. Mirzaei, M. Tahmasebi, J.T. Magee, *Acta Cryst. E* 76 (2020) 518–522.
- [45] G.A. Tsigdinos, *Boston University*, 1961.
- [46] L.J. Farrugia, *J. Appl. Cryst.* 30 (1997) 565.
- [47] L.J. Farrugia, *J. Appl. Cryst.* 32 (1999) 837–838.
- [48] G.M. Sheldrick, *Acta Cryst A* 64 (2008) 112–122.
- [49] G.M. Sheldrick, *Acta Cryst. A* 71 (2015) 3–8.
- [50] T. Mosmann, *J. Immunol. Methods* 65 (1983) 55–63.
- [51] Z. Chen, H. An, H. Zhang, Y.J.C. Hu, *CrystEngComm* 15 (2013) 4711–4720.
- [52] W.-. Q. Kan, J. Yang, Y.-. Y. Liu, J.-. F. Ma, *Dalton Trans* 41 (2012) 11062–11073.
- [53] J.L. Navarrete, V. Hernández, F. Ramírez, *Biopolymers* 34 (1994) 1065–1077.
- [54] H. An, L. Wang, Y. Hu, F. Fei, *Cryst. Eng. Comm.* 17 (2015) 1531–1540.
- [55] C. Li, W. Qi, H. Cao, Y. Qi, S. Zhang, S. Xu, J. Sun, S. Guo, *Biomed. Pharmacother.* 79 (2016) 78–86.